Received: 24 February 2017 | Revised: 9 May 2017 | Accepted: 17 May 2017

DOI: 10.1111/ffe.12649

SPECIAL ISSUE CONTRIBUTION

WILEY

Effects of inclusions on the very high cycle fatigue behaviour of steels

André Pineau | Samuel Forest

Centre des Matériaux, Mines ParisTech, UMR CNRS 7633, BP 87, 91003 Évry Cedex, France

Correspondence
André Pineau, Centre des Matériaux, Mines ParisTech, UMR CNRS 7633, BP 87, 91003 Évry Cedex, France.
Email: andre.pineau@ensmp.fr

Abstract

The very high cycle fatigue of high-strength steels and many other alloys is controlled by the initiation and the propagation of cracks initiated at nonmetallic inclusions. Tiny cracks are early initiated from these inclusions. They propagate very slowly in a specific zone located close to the inclusion and called the fine-grained area (FGA) or optical dark area. This area has a size of the order of that of the inclusion. The FGA is followed by the formation of conventional crack propagation area with the presence of striations in many cases. The details of initiation of these very high cycle fatigue cracks depend on the relative elastic and thermal properties of inclusions and matrix. The specificities of the FGA zone are dependent on the hydrogen segregated at the interface of the inclusions. An elasto-plastic finite element calculation is performed to determine the residual stresses in the vicinity of the inclusions and to evaluate the effect of residual stresses.

KEYWORDS

finite element calculations, inclusions, local stresses, very high cycle fatigue

1 | INTRODUCTION

Very high cycle fatigue (VHCF) origins in high-strength steels and other alloys are mostly nonmetallic inclusions. Several studies have been devoted to the initiation of fatigue cracks at inclusions (see, eg, Tanaka and Mura[1]). These premature fatigue crack initiation sites are due to the influence of local stresses associated with the difference in elastic and plastic properties and/or the difference in thermal dilatation coefficients between the matrix and the inclusions. In the vicinity of a nonmetallic inclusion at the fracture origin, an optically dark area[2] or a fine-grained area (FGA)[3] is observed to be formed as a rule inside a fish-eye mark, which represents the particular morphology associated with the mechanism of internal fatigue cracks especially at high number of cycles to failure. The creation of an FGA is usually related to the presence of hydrogen segregated at the interface between matrix and inclusions.[4] Figure 1 illustrates an example of a fish-eye mark in a high-strength steel and, at the vicinity of one inclusion, the formation of an FGA.[5]

From an analysis of several features involved in this mechanism of failure, such as the development of FGA, the threshold for pure fatigue propagation as a function of crack length and inclusions size, an expression was deduced to estimate the internal fatigue limit, that is, the stress level below in which fracture produced by cracks initiated from an internal inclusion is not found after a large number of cycles (approximately 10^{10} cycles)[6]:

$$\sigma_{\text{int}} = 444\ \Delta K_{\text{th}} / \sqrt{n\, R_{\text{i}}^{\max}}, \tag{1}$$

where ΔK_{th} is the pure fatigue crack propagation threshold, $R_{\text{i}}^{\max}$ is the radius of the maximum inclusion, and n has been added as "n" times the inclusion radius R_{i}, which could be equal to 2 as a first approximation, but it can be estimated according to the type of inclusion or the influence of the hydrogen content. Here it is important to mention that

 © 2017 Wiley Publishing Ltd.

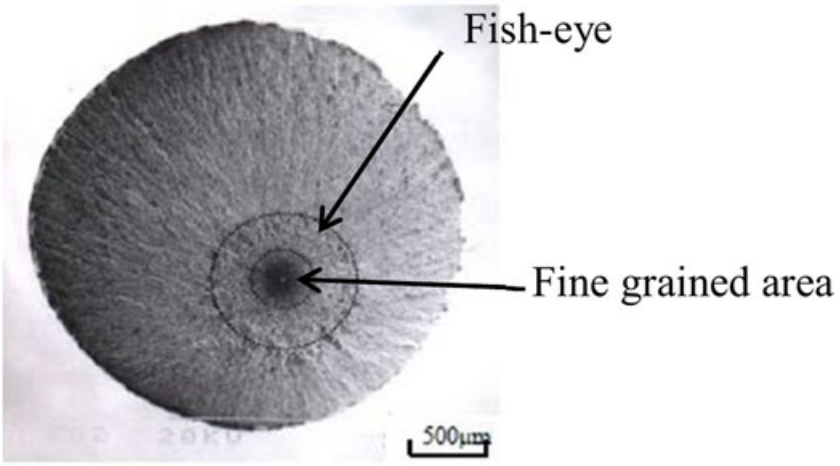

FIGURE 1 Fracture surface with a fish-eye in axial loading ($\sigma_a = 900$ MPa), $N_f = 1.94 \times 10^8$ cycles (refer to Sakai et al[3]) [Colour figure can be viewed at wileyonlinelibrary.com]

expression 1 is deduced from a pure fatigue crack propagation threshold concept and that the total fatigue life is considered to be similar to the number of cycles to create a crack with a length a_0^{pf} disregarding the number of cycles to propagate this crack to obtain the facture of the specimen. Crack initiation can be defined as the number of cycles used in the nucleation and propagation of the FGA. It represents a significant part of the fatigue life (approximately 90-95%), in particular at high cycle fatigue life.

2 | INCLUSIONS AND FGA

Over the past recent years, many aspects of the FGA have been studied, such as their morphology, their size, the stress intensity factor at their periphery, the mechanisms of their formation, their initiation, and their crack growth; see, eg, previous studies.[7-14]

We will concentrate on their formation and their growth behaviour. Simple models (Figure 2) to estimate the threshold nominal stress to initiate fatigue fracture from cracks initiated at internal inclusions have been proposed.[2,15,16] The defined internal fatigue resistance is obtained from (1) the threshold for pure fatigue crack propagation and (2) the inclusion size in the material where the crack takes place. The variation of the experimental trends of the relationship between fatigue resistance $\Delta\sigma_{aR}$ and tensile strength σ_u (for a load ratio $R = \sigma_{min}/\sigma_{max} = -1$) is shown in Figure 3.

It is well known that fatigue resistance σ_a increases with tensile strength σ_u (or with hardness, H_V). However, after a given tensile strength, the experimental σ_a-σ_u trend changes. The linear relationship usually observed between σ_a and σ_u at lower strength breaks down and σ_a decreases when σ_u is increased above a given value. This change in σ_a-σ_u relationship is associated with a modification of the fatigue life, which is related to surface fatigue crack initiation mechanisms, while at higher resistance, a fracture process given by an internal fatigue crack initiation defines the relation between σ_a and σ_u. This behaviour is illustrated in Figure 4. An example obtained on a high-strength steel (JOS SUJ2-QT) is shown in this Figure. The existence of 2 mechanisms gives an S-N curve with 2 knees (Figure 5). In this figure, the typical fracture surface appearance of both initiation zones associated with surface and internal initiation processes is also shown. In this article, we will deal only with internal initiation from inclusions, and we will concentrate essentially on VHCF.

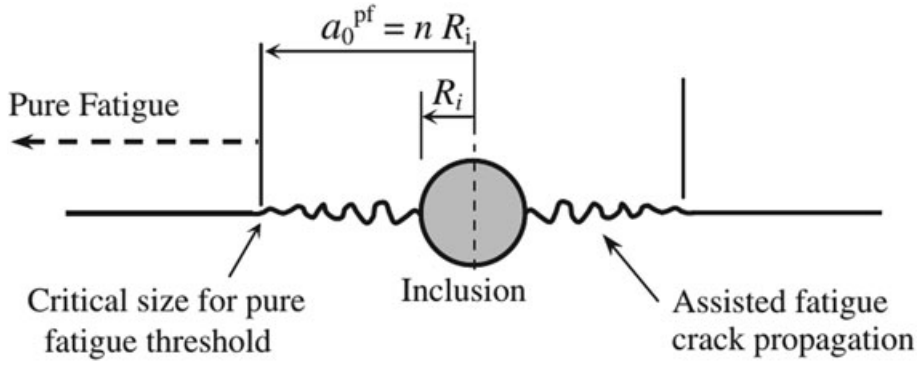

FIGURE 2 Schematic mechanism for very high cycle fatigue from internal inclusion with an initial assisted fatigue crack initiation and early propagation stage[4]

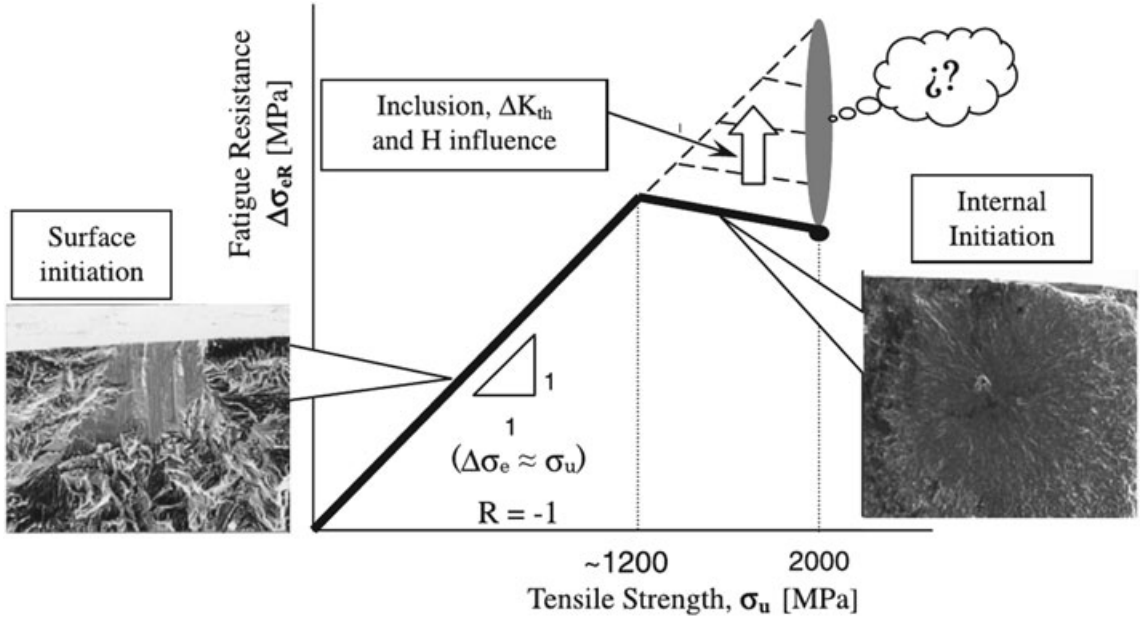

FIGURE 3 Experimental trends of the relationship between fatigue resistance $\Delta\sigma_{aR}$ and tensile strength σ_u for $R = -1$. Typical fractographic appearance of the initiation zones is also shown[4]

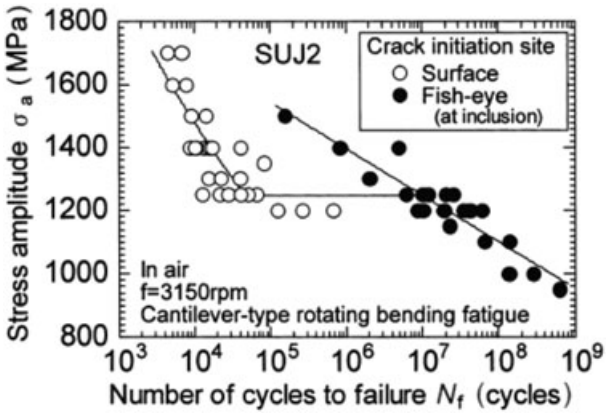

FIGURE 4 S-N curve of JIS SUJ2-QT steel[17]

The problem of VHCF is essentially that of small cracks, and the evidence of a tentative threshold step of the S-N diagram, which indirectly implies that the problem is one of crack propagation.[1,7,15] However, the crack growth rate in this regime is very low and smaller than the lattice spacing. Nevertheless, it is necessary to consider that for VHCF, the initiation and the early microcrack propagation are usually assisted by other mechanisms such as local residual stresses (see Section 6) and the presence of hydrogen around the inclusions. This zone in which propagation is assisted by other mechanisms, a_0^{pf}, is shown schematically in Figure 2. The critical crack length a_0^{pf} coincides with the radius of the FGA defined by Murakami.[2,16,18,19]

Among the factors affecting the crack initiation from inclusions, the inclusions type, shape and size (R_i), residual stresses, and hydrogen content play important roles. Examples of types of inclusions are Al_2O_3, Al_2O_3 (CaO), MnS, and TiN. The stress concentrations introduced by the inclusions should be taken into account. The effect of H_2 has been studied by several authors.[20,21]

The threshold for pure fatigue crack propagation, ΔK_{th}, is function of crack length because of the small size $\left(a_0^{pf}\right)$ of the cracks initiated from small inclusions. The following expression developed by Murakami et al[18,19] valid for load ratio $R = -1$ is expressed as

$$\Delta K_{th} = 3.3\times10^{-3}\,(H_V + 120)\left(\sqrt{area}\right)^{1/3}, \qquad (2)$$

where H_V is the Vickers hardness (kgf/mm^2) and *area* (in μm^2) is the area of the surface of the inclusion projected on a plane perpendicular to the maximum tensile stress; ΔK_{th} is in MPa m$^{1/2}$:

Equation 2 can also be written as a function of crack length:

$$\Delta K_{th} = 4\times10^{-3}\,(H_V + 120)a^{1/3}. \qquad (3)$$

The size of the assisted fatigue zone that defines a_0^{pf} has been established from results published in the literature[22]:

$$\sqrt{(area)_{FGA}}/\sqrt{(area)_{inclusion}} = a_0^{pf}/R_i = 0.25N^{0.125}. \qquad (4)$$

Using the above expressions, it was shown by Chapetti et al[23] that the fatigue endurance stress, $\Delta\sigma_{th}$, the number of cycles

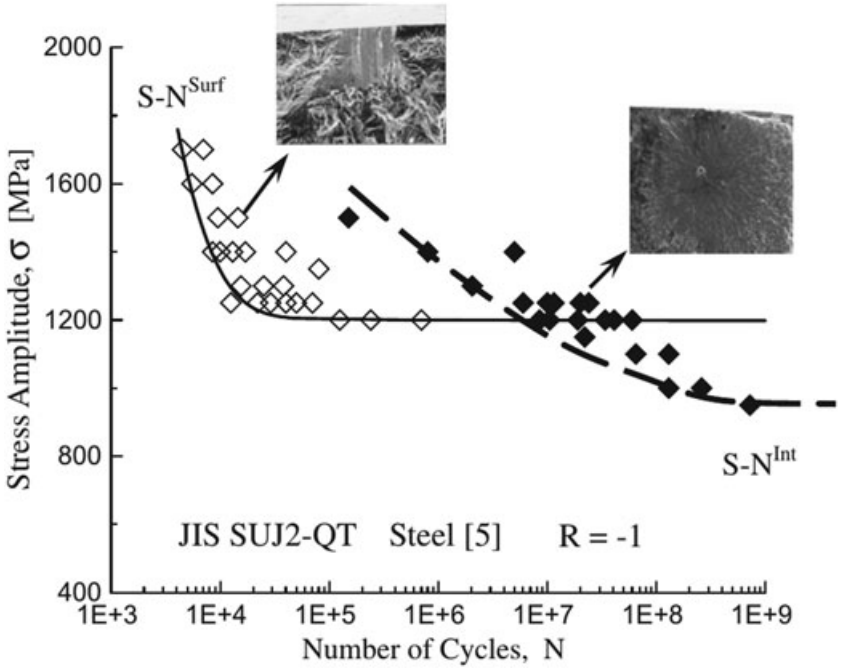

FIGURE 5 S-N curve giving the applied nominal stress as a function of the number of load cycles to failure *N*, for a JIS SUJ2-QT steel[4]

necessary to propagate the crack from a_0^{pf}, was related to the following equation:

$$\Delta\sigma_{th}\, N^{1/48} = 4.473\ (H_V + 120)/(R_i)^{1/6}. \qquad (5)$$

To define the value of R_i, it has been shown that it is necessary to take into account the influence of the statistical size distribution of inclusions.[22]

The variation of the fatigue threshold as a function of $(area)^{1/2}$ parameter for 2 steels with different hardness is shown in Figure 6. Even though expression 2 seems to work well till a value of $(area)^{1/2}$ of 1000 μm for low strength steels, the crack length [or the value of $(area)^{1/2}$] at which the fatigue threshold for short cracks equals the threshold for long cracks (ΔK_{thR}) depends on the materials: the higher the strength of the material, the shorter the crack length for transition. Chapetti[4] has shown that the trend for the threshold as a function of tensile strength for load ratios *R* equal to 0.1 and −1 can be expressed as

$$\Delta K_{th0.1} = -0.0021\sigma_u + 8.4 \qquad R = 0.1, \qquad (6)$$

$$\Delta K_{th-1} = -0.0038\sigma_u + 15.5 \qquad R = -1, \qquad (7)$$

with σ_u in MPa, and $\Delta K_{th0.1}$ and ΔK_{th-1} in MPa $m^{1/2}$.

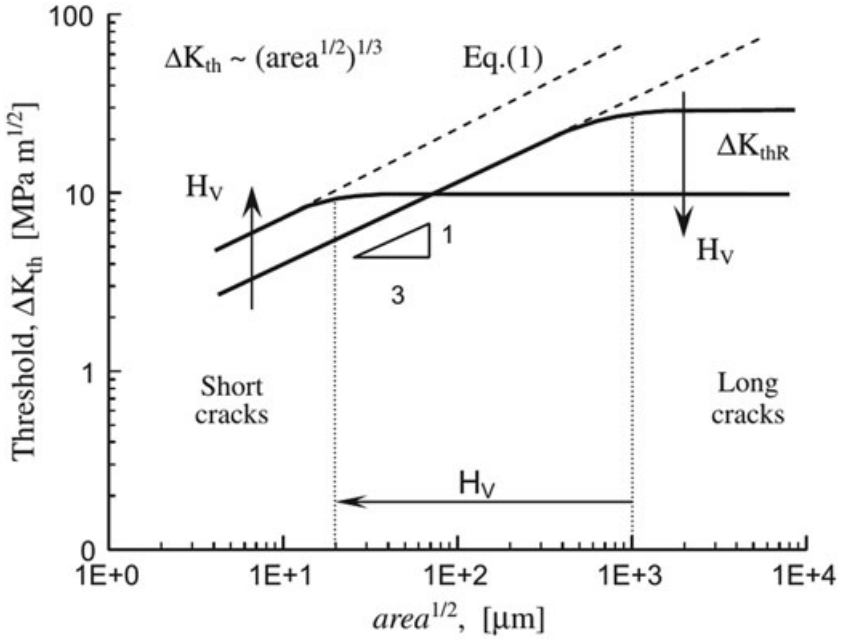

FIGURE 6 Fatigue threshold as a function of $(area)^{1/2}$ parameter for 2 steels with different strengths[4]

3 | INTERNAL FATIGUE RESISTANCE FOR VERY HIGH CYCLE FATIGUE

A simple model to estimate the threshold nominal stress to obtain fracture from cracks initiated at internal inclusions has been proposed by Bathias and Paris,[15] by using the threshold for pure fatigue crack propagation and the inclusion size in the material from which the crack initiates. The internal pure fatigue resistance associated with given internal inclusion can be established with Equation 8 (refer to Frost et al[24]):

$$\Delta K = 2/\pi \times \Delta\sigma\sqrt{\pi a}, \tag{8}$$

with the applied ΔK equal to the pure fatigue crack propagation threshold ΔK_{th} for a given crack length. With $\Delta K = \Delta K_{th}$, $a = n\,R_i$ and $\Delta\sigma = 2\sigma_a^{int}$, we obtain the following expression to estimate the fatigue resistance associated with internal initiation:

$$\sigma_a^{int} = \Delta K_{th}/\sqrt{nR_i}, \tag{9}$$

where the radius R_i is in μm and ΔK_{th} is given by the lower value from expressions 3 and 7 in MPa $m^{1/2}$. The value of n can be taken as follows:

$$n = R_{FGA}/R_i = 0.25N^{0.125}. \tag{10}$$

4 | ESTIMATION OF CRACK GROWTH LAW

Kuroshima and Harada[25] reported that a fatigue crack was formed from inclusions inside the specimen of high-strength steel at a very early stage of fatigue life.

Figure 7 from Tanaka and Akiniwa[26] illustrates the crack propagation rate and the stress intensity range for surface cracks and internal cracks in a bearing steel. The solid line

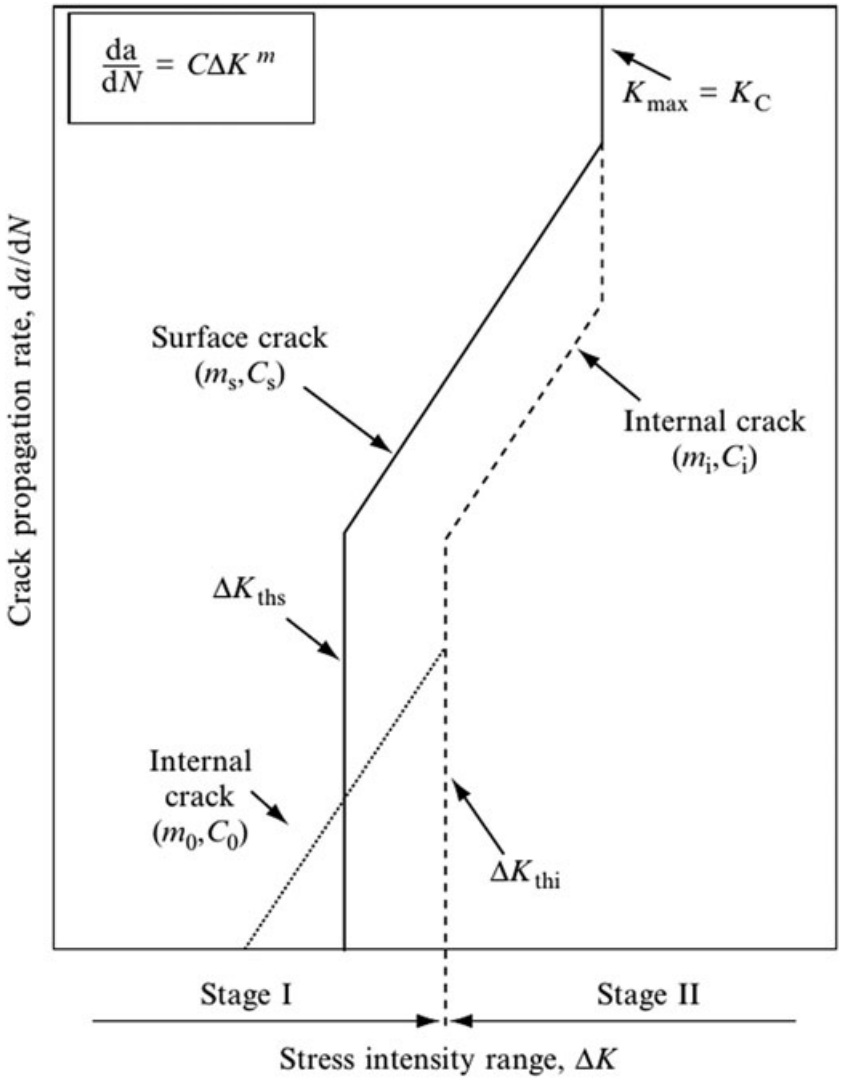

FIGURE 7 Fatigue crack growth law for bearing steel[26]

shows the relation between the crack propagation rate and the stress intensity range for surface cracks. This relation is a simplification of the conventional through-crack propagation law. The fatigue crack does not propagate below the threshold value ΔK_{ths}, and unstable fracture takes place at the maximum stress intensity factor equal to the fracture toughness K_C. In between the following power law holds:

$$da/dN = C_S \Delta K^{ms}, \quad (11)$$

where C_S and ms are material constants.

When a similar law is applied to internal cracks, the relation is shown with a dashed line in Figure 7 where the corresponding threshold is denoted by ΔK_{thi}. Murakami et al[16] suggested that hydrogen trapped at inclusions enhanced the propagation of these small cracks. Here we assume the following propagation law:

$$da/dN = C_0 \Delta K^{n0}, \quad (12)$$

and it is drawn with the dotted line in Figure 7. This diagram for internal crack propagation is similar to the diagram proposed by Kuroshima and Harada.[25]

The fatigue crack does not propagate below the threshold value ΔK_{ths} (cracks initiated at the surface), and unstable fracture takes place at the maximum stress intensity factor equal to the fracture toughness. In between the following law

$$da/dN = C_S \Delta K^{m}, \quad (13)$$

holds.

The above relation is not enough to explain the propagation of small internal cracks. Even when the crack is below the threshold, it can still propagate as indicated schematically by the dotted line, and the crack propagation rate can be expressed as

$$da/dN = C \Delta K^{m0}, \quad (14)$$

The diagram for internal crack propagation is similar to the one proposed by Kuroshima and Harada.[25] In a study devoted to a bearing steel, Tanaka and Akiniwa[26] have found that $\Delta K_{ths} = 2.65\ MPa^{1/2}$ while $\Delta K_{thi} = 4.0 MPa^{1/2}$. Several reasons have been invoked to explain why $\Delta K_{ths} \ll \Delta K_{thi}$:

- The inclusions may have an irregular shape, which produces stress concentration. They may also be chemically inhomogeneous.
- Cyclic work softening on high-strength steels due to local plasticity.
- Local ratcheting effect in relation with constitutive equation.
- Difference in elastic modulus between the matrix and the inclusions.
- Hydrogen embrittlement.[19,27]

5 | INCLUSIONS PROPERTIES AFFECTING FATIGUE RESISTANCE

The effect of an inclusion on the fatigue properties depends on its size, shape, thermal, and elastic properties and its adhesion to the matrix. These factors are related to the stress concentration and the stress distribution around the inclusion.[28]

5.1 | Inclusion size

Inclusion size has a major effect on the fatigue properties. The distribution of inclusions in metals is usually experimental.[18] Critical inclusion size is dependent on the strength and hardness of the material. In the investigations of Nishijima et al[29] on tempered martensitic steels with a tensile strength range of 700 to 1300 MPa, the virtual size of inclusions was approximately 45 μm in the rotating bending tests. Melander and Ölund[30] reported that T_i(CN) inclusion and alumina inclusions as small as 3 to 17 μm were found on the fracture surface of rotating bending fatigue test specimens of bearing steels. It was also concluded that T_i(CN) inclusions were detrimental to fatigue life as oxide inclusions of approximately 3 times their size.

5.2 | Inclusion shape

Inclusions with an irregular shape and sharp edges produce larger stress concentrations around the inclusions than particles with a smooth shape. These irregular shapes make it easier for a fatigue crack to initiate. For example, T_i(CN) inclusions having a sharp angular shape cause earlier crack initiation than the globular inclusions that have the same size.

5.3 | Thermal properties

Differences in the thermal expansion coefficients of the inclusion and the matrix can generate internal stresses around inclusions. These thermal stresses can be generated during the cooling after hot rolling or during the thermal heat treatment of quenching and tempering. In Figure 8,[31] the tendency for forming thermal internal stresses is presented for different inclusion types in a 1% C-Cr bearing steel.[31-34] It can be seen in Figure 8 that sulphides give rise to voids at the interface between inclusion and matrix where most oxides cause dilatational stresses. These stresses may greatly alter the properties of the matrix and localised yielding may occur.

5.4 | Elastic properties

When Young's modulus of an inclusion is greater than Young's modulus of the matrix, eg, for T_iC, Al_2O_3, and calcium aluminates, a stress concentration is generated around

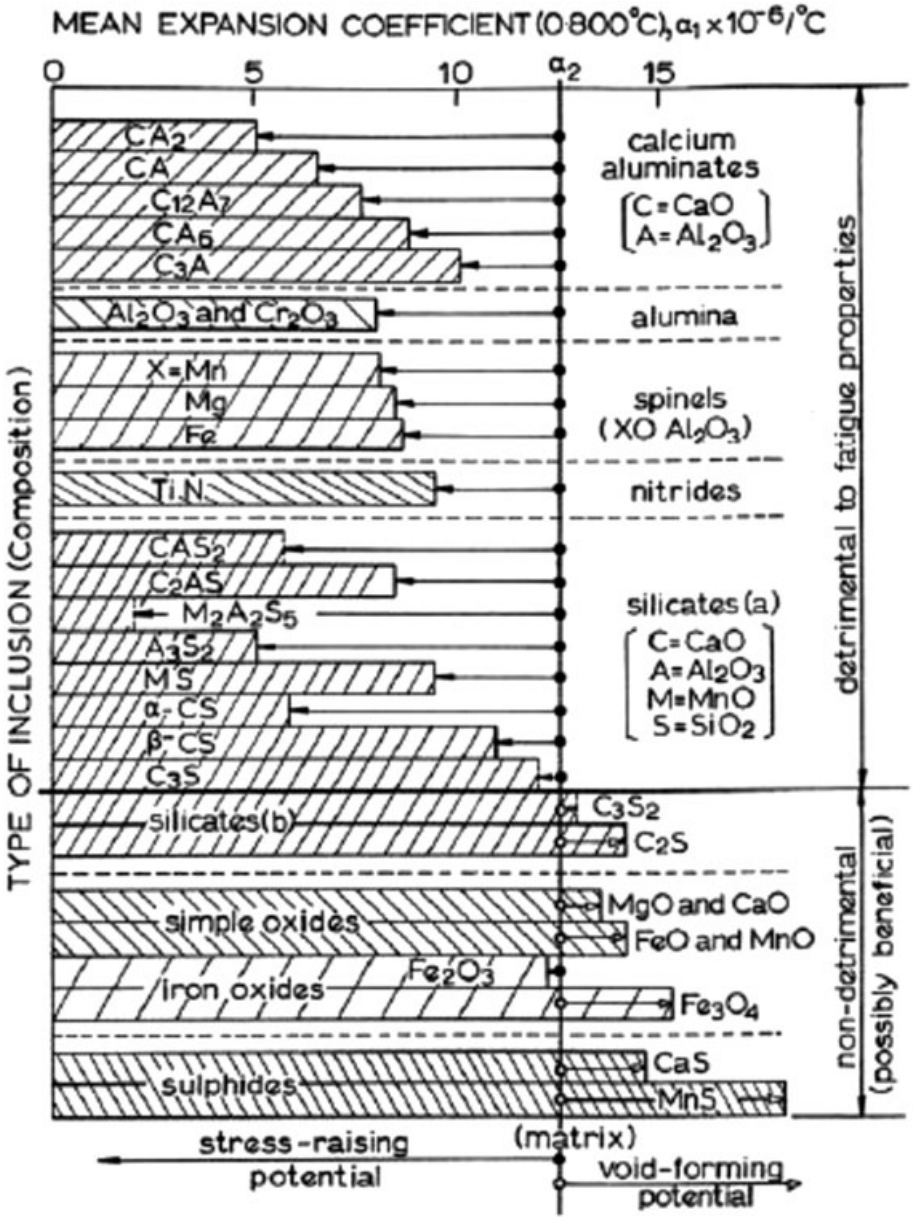

FIGURE 8 Stress raising properties of various inclusion types in 1% C-Cr bearing steel[31]

the inclusion under a tensile stress. Young's modulus of the sulphides is usually lower than that of the matrix, which makes sulphides relatively harmless. Hard inclusions with low deformability may cause microcrack formation at the interface when the material is hot rolled. A fatigue crack may initiate from these microcracks. Thermal and elastic properties of various inclusion types are presented in Table 1.[31-34]

5.5 | Adhesion to the matrix

The adhesion of the inclusion to the matrix is not always perfect, which facilitates the initiation of a tiny crack from the interface. Fatigue cracks may also initiate through the inclusion, ie, the inclusion cracks, or it may initiate from the interface between the different phases of an inclusion. The fatigue crack initiation is usually faster in the cases where a crack initiates from a cracked inclusion than in the cases where a crack initiates from the interface between the inclusion and the matrix. It should be emphasised that all the finite element calculations presented in the above literature[30-35] have been made in elasticity. The introduction of plasticity is made in the following section.

6 | FINITE ELEMENT ANALYSIS OF PLASTIC STRAIN ACCUMULATION AT INCLUSIONS

The accumulation of plastic strain around undamaged inclusions plays a major role on crack initiation under HCF

TABLE 1 Various types of inclusions in steels[28]

Inclusion Type	Inclusion	$\alpha \times 10^{-6}$, °C	E, GPa	ν
Sulphides	MnS	18.1	(69-138)	(0.3)
	CaS	14.7		
		8.8		
Calcium aluminates	$CaS–6Al_2O_3$	5.0	(113)	(0.234)
	$CaS–2Al_2O_3$	6.5		
	$CaO–Al_2O_3$	7.6		
	$12CaO–7Al_2O_3$	10.0		
	$3CaO–Al_2O_3$			
Spinels	$MgO–Al_2O_3$	8.4	271	0.26
	$MnO–Al_2O_3$	8.0		
	$FeO–Al_2O_3$	8.6		
Alumina	Al_2O_3	8.0	389	0.25
	Cr_2O_3	7.9		
Nitrides	TiN	9.4	(317)	(0.192)
Oxides	MnO	14.1	(178)	(0.306)
	MgO	13.5	306	0.178
	CaO	13.5	183	0.21
	FeO	14.2		
(Matrix)				
1% C, 1.5% Cr	(850°C → Ms)	(23.0)		
		(10.0)		
	(M_f → R.T.)			
	$\gamma \rightarrow a'$	12.5	206	0.29
	(850°C → R.T.)			

loading conditions. This microplasticity results from the stress concentration induced by the elastic mismatch between the inclusion and the matrix. Even though the overall loading is below the macroscopic yield stress of the material, plasticity events can occur at some locations around the inclusion. Depending on the cyclic hardening behaviour of the matrix, 3 main situations arise in the vicinity of the inclusion: elastic shakedown, elastic-plastic accommodation including dissipation effects at each cycle, and, possibly, ratcheting phenomena leading to the progressive accumulation of plastic strain.[36] The 2 latter cases may result in early crack initiation.

Surprisingly enough, only few studies are devoted to the detailed computational analysis of cyclic plasticity around inclusions for large numbers of cycles. Contributions dealing with metal matrix composites concentrate on homogenisation methods for the derivation of effective viscoplastic constitutive laws at the macroscopic scale,[37] including macroscopic ratcheting effects induced by asymmetric loading in the work of Guo et al.[38] Fleming and Temis[39] investigate the competition between interface debonding and crack initiation in the matrix induced by local ratcheting. Their analysis is based on finite element simulations of the cyclic response of a spherical inclusion embedded in a matrix displaying isotropic hardening. Their computations show the complexity of the plastic strain field distribution and redistribution during cycling loading, and the need for a very fine finite element mesh for correct description of the maximum of accumulated plastic strain at about 45° from the tensile axis close to the matrix-inclusion interface. The complex plastic zones were recently studied around elliptical particles for which stress concentration effects are enhanced.[40]

However, the systematic dependence of plastic strain accumulation on matrix work-hardening, inclusion-matrix elastic mismatch, residual stresses, and its relation to fatigue crack initiation and crack path around the inclusion remains to be studied computationally, prior to direct experimental observations.

The objective of this section is to unveil some aspects of such an analysis, leaving the systematic study for future work. For that purpose, the problem of one single elastic inclusion embedded in a practically infinite elastic-plastic matrix under cyclic loading is solved using the finite element method with the code Zset.[41]

6.1 | Materials and loading characteristics

The considered matrix material has characteristics close to that of a maraging steel (Young's modulus, 200 GPa; Poisson ratio, 0.3; yield stress, R0 = 1 GPa). The von Mises criterion is used, and 2 types of hardening laws are considered. Isotropic hardening describes the evolution of the yield stress, R, as a function of cumulative plastic strain variable p. An exponential function is chosen:

$$R(p) = R0 + Q(1-\exp(-bp)). \quad (15)$$

$Q = 400$ MPa and $b = 1000$ are the matrix isotropic hardening parameters.

Alternatively, kinematic hardening according to the Armstrong-Frederick law is chosen[42]:

$$\dot{X} = \frac{2}{3} C \dot{\epsilon}^p - D\dot{p} X \quad \text{and} \quad f(\sigma, X, R) = \sqrt{\frac{3}{2} (S-X) : (S-X)} - R(p), \tag{16}$$

where $C = 400$ GPa and $D = 1000$ are the kinematic hardening parameters.

Note that the parameters are such that the isotropic and kinematic hardening laws lead to the same tensile curve, but to distinct cyclic loops.

Two values of the elastic mismatch between inclusion and matrix are considered, 2 and 0.5, corresponding to hard and soft inclusions, respectively.

The 2D finite element computations are performed using quadratic axisymmetric elements with reduced integration. Implicit Newton solvers are used at the global and local levels.[42]

A stress-controlled uniaxial test is simulated with alternating stress levels +950 MPa and −950 MPa applied as a far field in the matrix. The chosen load is smaller than the yield stress so that plasticity occurs only in the neighbourhood of the inclusion, as it is the case in HCF. The loading direction is axis 2 of the used coordinate frame. The fields of plastic deformation shown in the following are provided after 20 cycles, at the maximal load of the cycle, if not otherwise stated.

6.2 | Isotropic vs kinematic hardening effect

The distribution of the Euclidean norm of the plastic strain tensor, called equivalent plastic strain, is shown in the matrix surrounding the hard and soft inclusions in Figures 9A,B and 10A,B, respectively. After 20 cycles, this distribution does

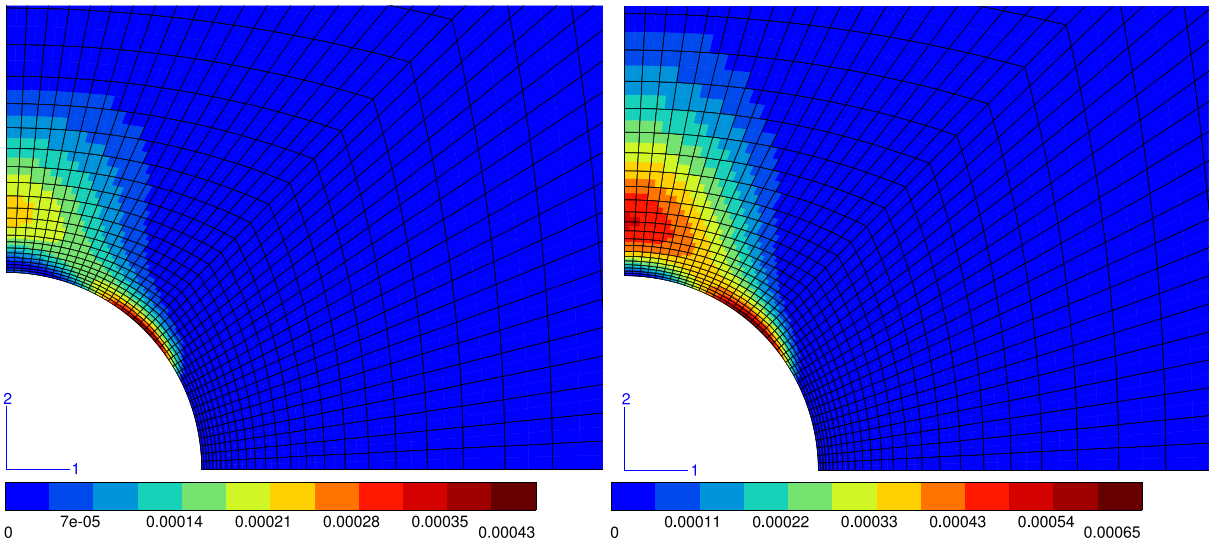

(A) isotropic hardening

(B) kinematic hardening

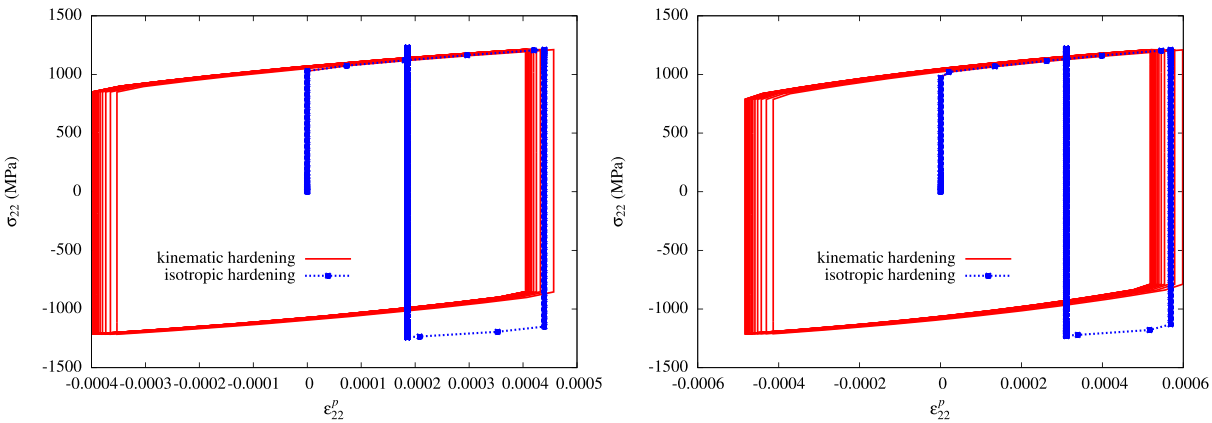

(C) material point in the frontal zone

(D) material point in the interface zone

FIGURE 9 A-B, Contour maps of the equivalent plastic strain around a hard inclusion for 2 types of strain hardening laws. C-D, Comparison of the axial stress-plastic strain loops for 2 hardening laws in 2 regions of the matrix [Colour figure can be viewed at wileyonlinelibrary.com]

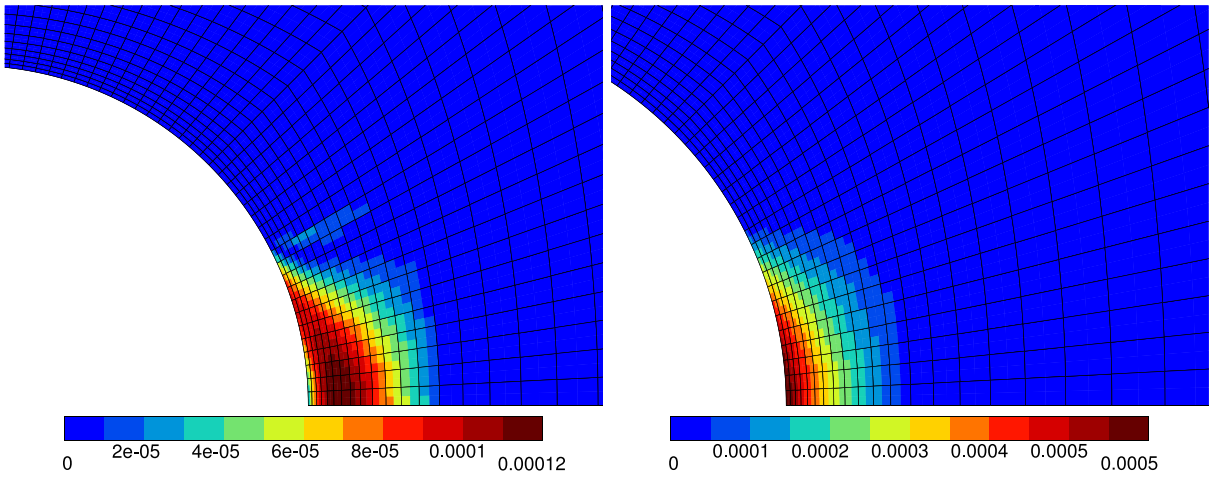

(A) isotropic hardening (B) kinematic hardening

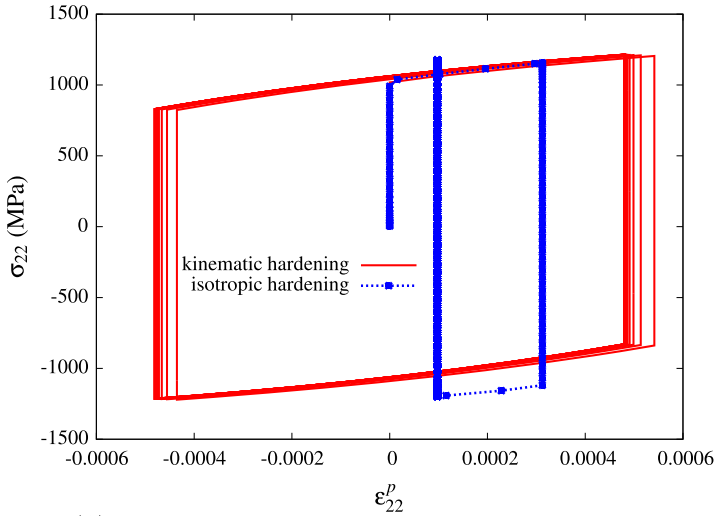

(C)

FIGURE 10 A-B, Contour maps of the equivalent plastic strain around a soft inclusion for 2 types of strain hardening laws. C, Comparison of the axial stress-plastic strain loops for 2 hardening laws at the location of maximal plastic activity in the matrix (at or close to the equator) [Colour figure can be viewed at wileyonlinelibrary.com]

not evolve significantly. For the hard inclusion in a matrix endowed with isotropic hardening, the result presented by Fleming and Temis[39] is retrieved. Two zones of maximal plastic strain are observed: one at the interface between the matrix and the inclusion at about 45°, and the other inside the matrix at some distance of the interface along the tensile axis. The latter zone is called the frontal zone in the work of Fleming and Temis.[39] This name is kept in this work. The plastic strain is found to be significantly higher in the interface zone than in the frontal domain. In contrast, kinematic hardening leads to a more balanced distribution among both locations. The plastic strain reached locally is higher in the kinematic hardening case. This is because isotropic hardening leads to elastic shakedown after 1 cycle in both locations (Figures 9C,D and 10C), whereas elastic-plastic accommodation is observed for kinematic hardening. Some ratcheting can be observed before stabilisation of the plastic strain-stress loops in this case. It follows that dissipation will continue during the following cycles, thus promoting crack initiation at the interface or in the frontal zone. Note that the plastic strain amplitude is larger close to the interface, suggesting crack initiation at this location rather than the frontal zone.

The situation is quite different in the presence of a soft inclusion (Figure 9). Only one zone of maximal plastic strain is observed at the equator. It lies at the interface in case of kinematic hardening and at a distance from the interface on the ligament for isotropic hardening.

Note that the plastic strain amplitudes are slightly smaller in the soft inclusion than in the hard inclusion.

The detailed description of the locations of plastic activity during cycling loading gives indications about the possible crack initiation points: at the interface at 45°, or possibly in the frontal zone (close to the pole), for the hard inclusion, and at the equator or slightly ahead for the soft

inclusion. It may also have further implications on the crack path during the propagation stage.

6.3 | Effect of cyclic softening

Many high-strength engineering alloys display cyclic softening, ie, a decrease of the stress amplitude with the number of cycles for strain-controlled uniaxial fatigue, eg, IN718 superalloy[43] and maraging steels.[44] The stress amplitude generally saturates before crack initiation. The cyclic hardening curve then lies below the monotonic tensile curve.[43] This feature is shown in this section to have dramatic effects on the plastic strain distribution around an inclusion. A simple constitutive model is chosen to represent monotonic hardening and cyclic softening in the matrix material. It combines an isotropic softening component and a kinematic hardening variable with the following values of the parameters:

$$R0 = 1600 \text{ MPa}, \quad Q = -1000 \text{ MPa}, \quad b = 3, \\ C = 400 \text{ MPa}, \quad D = 1000. \tag{17}$$

The yield stress has been enhanced compared to that of the previous section. Because of isotropic softening, this value decreases towards 600 MPa at a rate dictated by the parameter b in the exponential function of Equation 15. The kinematic hardening can add 400 MPa when it is saturated. It ensures convex cyclic loops usually observed for these materials.

Figure 11A,B shows the equivalent plastic strain distribution after 30 and 50 cycles, respectively. After 30 cycles, the

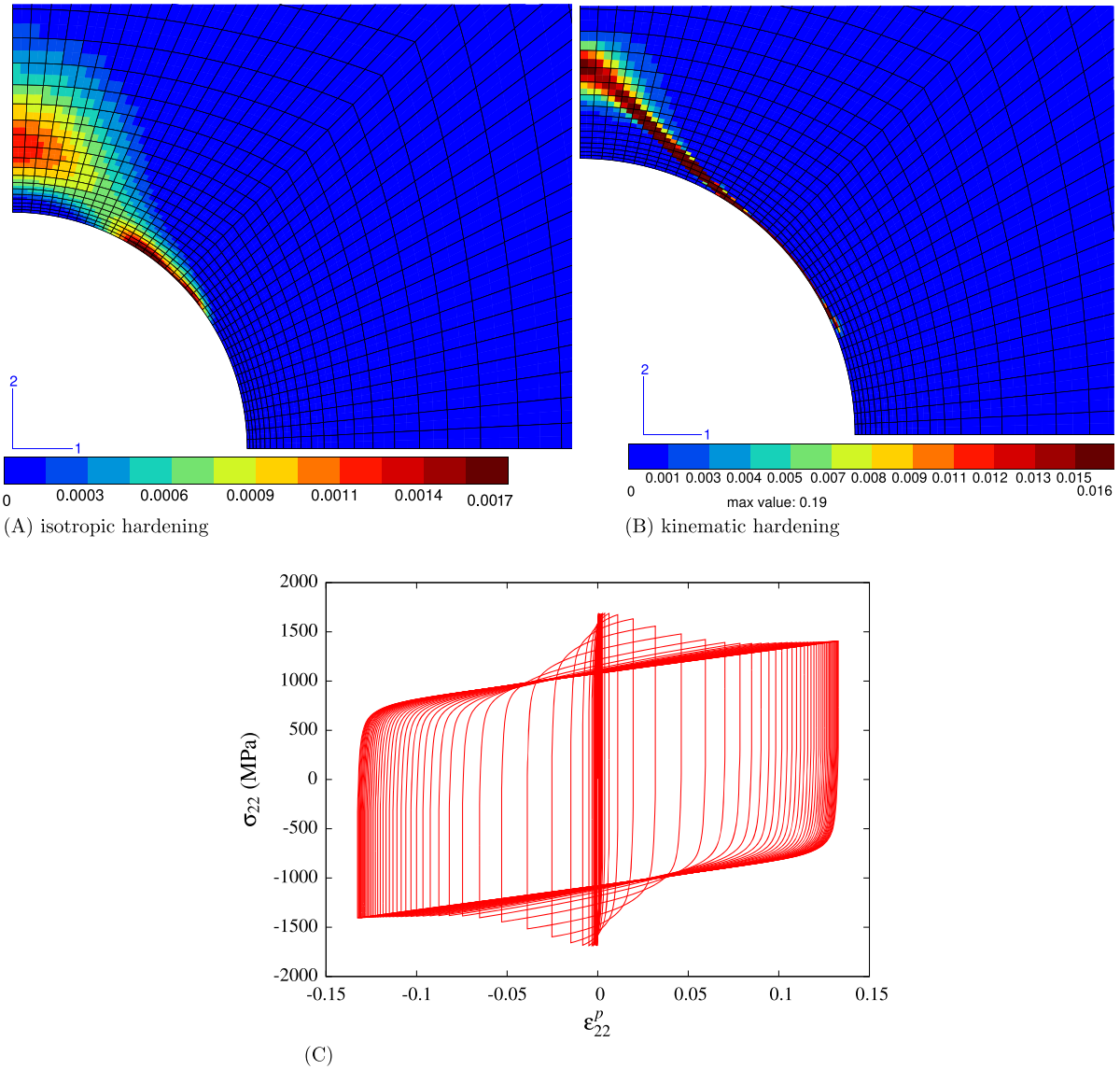

FIGURE 11 Effect of cyclic softening behaviour on the plasticity around the inclusion: plastic strain localisation after A 30 cycles and B 50 cycles. C, Stress-plastic strain loops at a material point located close to the interface at 45° (hard inclusion) [Colour figure can be viewed at wileyonlinelibrary.com]

distribution is similar to that of Figure 9B with maximal values in the frontal and interface zones. This distribution is then found to evolve dramatically towards plastic strain localisation into an intense slip band connecting the frontal zone to the interface region. Plastic strain reaches very high values, larger than 10%, inside this sharp band, especially in the first layer of elements at the interface at about 45° (Figure 11B). Some mesh dependence of the results is expected in the simulation, with thinner band width and higher strain level inside the band when finer meshes are used. The cyclic response of a material point located in this strain localisation zone is given in Figure 4C. The stress vs plastic strain loops are shown to widen considerably to reach almost stabilised loops with amplitude of more than 20% plastic strain. The first loops are high and thin, whereas the final ones are wide and display smaller stress amplitude.

Such localisation phenomena in heterogeneous materials under cycling loading have not been studied from the computational mechanics perspective nor compared to experimental evidence yet, to the knowledge of the authors.[45] They may be responsible for early crack initiation at the interface and subsequent straight crack propagation.

6.4 | Effect of residual stresses

The previous simulations do not account for the presence of residual stresses induced by the thermal expansion mismatch between the matrix and the inclusion during cooling from high temperature processing. Residual stresses are known to significantly affect the subsequent fatigue behaviour of metal matrix composites. The impact of residual stresses on the plastic strain distribution around the inclusion after cycling

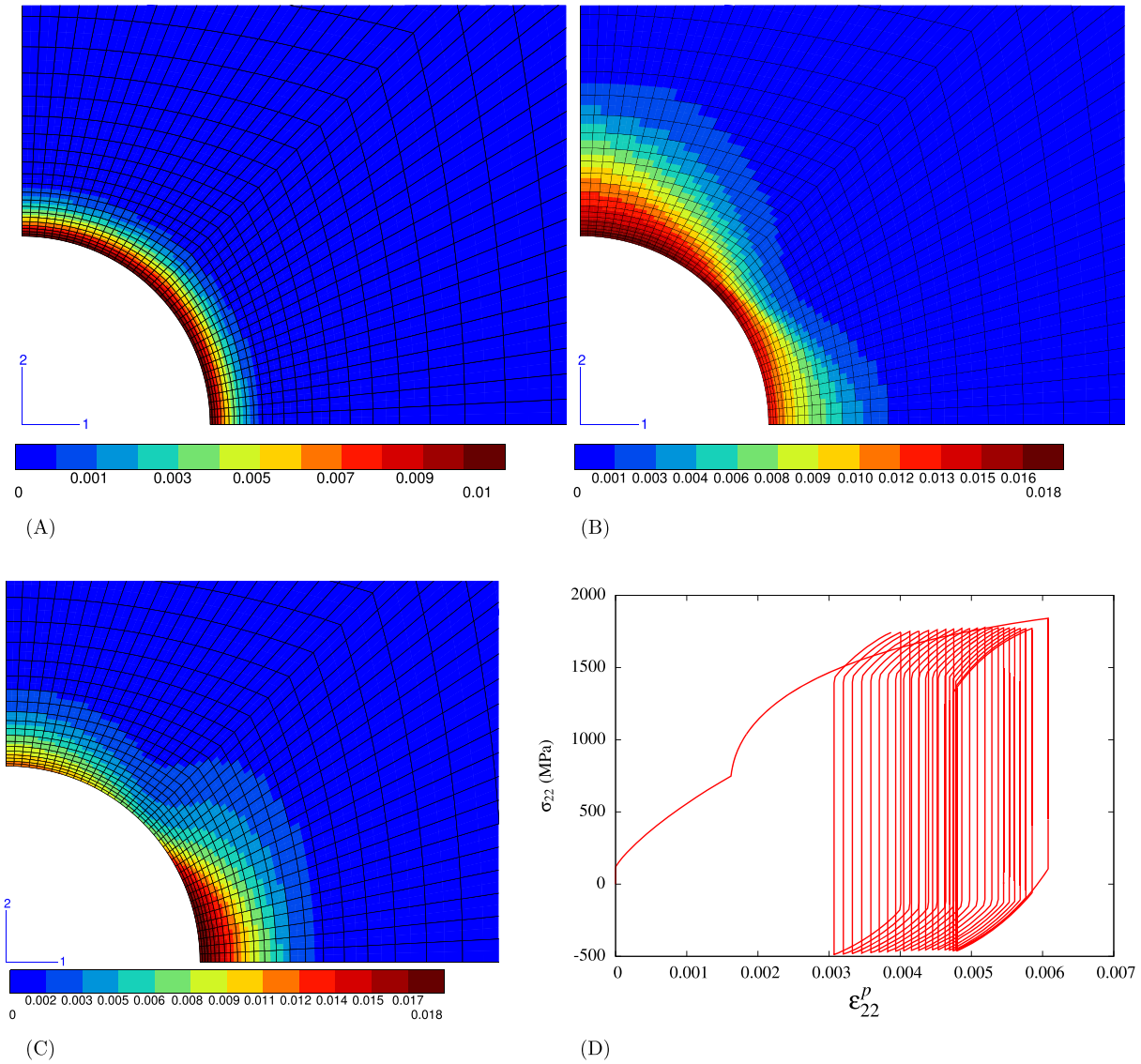

FIGURE 12 Effect of residual stresses on plastic strain distribution: A, residual equivalent plastic strain field after cooling (hard inclusion); B, equivalent plastic strain field after 20 cycles loading (hard inclusion); C, equivalent plastic strain field after 20 cycles loading (soft inclusion); D, stress-plastic strain loop at a material point located close to the interface at 45° (hard inclusion) [Colour figure can be viewed at wileyonlinelibrary.com]

is illustrated in this section on the basis of the introduction of a thermal strain in the inclusion. The inclusion thermal expansion coefficient is assumed to be constant with the typical value of 10e−5/K, according to Table 1. A cooling from 800°C to room temperature is simulated first. For simplicity, the temperature and time dependence of the matrix behaviour are not accounted for. The simple kinematic hardening law considered in the previous section is used in the matrix. Figure 4A shows the equivalent plastic strain around the inclusion, as predicted by the model after cooling. Plastic strain values of 1% are reached close to the interface because of the bonding between the contracting inclusion and the metal matrix. Twenty cycles of stress-controlled loading are then applied to the composite with residual stresses. The plastic strain distribution of Figure 12B is found to differ significantly from that of Figure 9B. Plastic flow is found to occur all around the inclusion during cyclic loading, in contrast to the initial stress-free situation where plasticity is confined to the frontal and interface zones. Similar observations are made in the case of a soft inclusion with the same thermal expansion as the previous hard inclusion, even though plastic activity is stronger at the equator; see Figure 12C.

The axial stress-plastic strain response of a material point located close to the interface with a hard inclusion at 45° is shown in Figure 12D. The first loading branch up to 0.2% plastic strain corresponds to the cooling process. This branch is followed by the first loading in the first cycle up to 0.5% plastic strain. Subsequent fatigue loops exhibit a ratcheting effect towards smaller plastic strain levels. The loops are not saturated after 20 cycles, but it is anticipated that the loops will evolve towards a more symmetric loop in maximal and minimal stress values. This long ratcheting period is accompanied with dissipation and a lot of plastic activity, which play an essential role in possible crack initiation.

7 | CONCLUSIONS

In VHCF, cracks are initiated from tiny inclusions and propagate first in the FGA with a characteristic aspect. The end of the FGA is limited to the fish-eye mark.

The fatigue threshold of the crack initiated from the inclusion is smaller than the threshold for pure fatigue crack propagation[46,47]. This represents a significant part of the fatigue life (approximately 90-95%).

Estimations of crack growth laws are given in fracture mechanics concepts.

The nature of the inclusions affecting fatigue resistance is given. The most influent parameters are their size, their elastic properties, and their adhesion to the matrix.

Finite element calculations are used to evaluate the accumulation of plastic strain at inclusions. These calculations are performed with elastic inclusions and elasto-plastic matrix. Isotropic hardening and kinematic plastic hardening are considered. The effects of cyclic softening and residual stresses are also analysed. The deleterious effect of cyclic softening is shown.

Open issues remain like the role of hydrogen in the initiation and propagation of fatigue crack. The existence of a critical hydrogen content at the matrix-inclusion interface by introducing interface embrittlement in the finite element approach. The interface embrittlement is also controlled by the microplasticity close to the interface. The competition between plastic accumulation and interface debonding can be simulated by means of a cohesive-zone model combined with elasto-plasticity. Unfortunately, only limited information is available about actual values for such a hydrogen content threshold and the dependence on dislocation density.

REFERENCES

1. Tanaka K, Mura T. A theory of fatigue crack initiation at inclusions. *Metall Trans A*. 1982;13A:117-123.
2. Murakami Y, Nomoto T, Ueda T. On the life-controlling microstructural fatigue mechanisms in ductile metals and alloys on the gigacycle regime. *Fatigue Fract Eng Mater Struct*. 1999;22:581-590.
3. Sakai T, Sato Y, Oguma N. Characteristic S-N properties of high-carbon-chromium-bearing steel under axial loading in long-life fatigue. *Fatigue and Fracture of Eng Mater Struct*. 2002;25:765-773.
4. Chapetti MD. A simple model to predict the very high cycle fatigue resistance of steels. *Int. J. Fatigue*. 2011;33:833-841.
5. Chapetti MD. Prediction of threshold for very high cycle fatigue ($N > 10^7$ cycles). *Procedia Engineering*. 2010;2:257-264.
6. Chapetti MD, Tagawa T, Miyata T. Ultra-long cycle fatigue of high-strength carbon steels part I: review and analysis of the mechanism of failure. *Mat Sci Eng*. 2003;A356:227-235.
7. Sander M, Müller T, Lebahn J. Influence of mean stress and variable amplitude loading on the fatigue behaviour of a high-strength steel in VHCF regime. *Int J Fatigue*. 2014;62:10-20.
8. Ogawa T, Stanzl-Tschegg S, Schonbauer B. A fracture mechanics approach to interior fatigue crack growth in the very high cycle regime. *Eng Fract Mech.* 2014;115:241-254.
9. Hong Y, Lei Z, Sun C, Zhao A. Propensities of crack interior initiation and early growth for very-high cycle fatigue of high strength steels. *Int J Fatigue*. 2014;58:144-151.
10. Stanzl-Tschegg S. Very high cycle fatigue measuring techniques. *Int J Fatigue*. 2014;60:2-17.
11. Sakai T, Oguma N, Morikawa A. Microscopic and nanoscopic observations of metallurgical structures around inclusions at interior crack initiation site for a bearing steel in very high-cycle fatigue. *Fatigue Fract Eng Mater Struct*. 2015;38:1305-1314.
12. Chai G, Forsman T, Gustavsson F, Wang C. Formation of fine grained area in martensitic steel during very high cycle fatigue. *Fatigue Fract Eng Mater Struct*. 2015;38:1315-1323.

13. Hong Y, Liu X, Lei Z, Sun C. The formation mechanism of characteristic region at crack initiation for very-high-cycle fatigue of high-strength steels. *Int J Fatigue*. 2016;89:108-118.
14. Mayer H. Recent developments inn ultra-sonic fatigue. *Fatigue Fract Eng Mater Struct*. 2016;39:3-28.
15. Bathias C, Paris PC. In: Dekker M, ed. *Gigacyclic Fatigue in Mechanical Practice*. NY 10016, USA: CRC Press; 2005.
16. Murakami Y, Namoto T, Ueda T, Murakami Y. On the mechanism of fatigue failure in the superlong life regime ($>10^1$ cycles). Part I: influence of hydrogen trapped by inclusions. *Fatigue Fract Eng Mater Struct*. 1999;23:893-902.
17. Shiozawa K, Lu L, Ishihara S. S-N curve characteristics and subsurface crack initiation behaviour in ultra-long fatigues of a high carbon-chromium bearing steel. *Fatigue Fract Eng Mater Struct*. 2001;24:781-790.
18. Murakami Y, Endo M. Effect defects, inclusions and inhomogeneities on fatigue strength. *Int J Fatigue*. 1994;16:163-182.
19. Murakami Y. *Metal Fatigue: Effect of Small Defects and Non-metallic Inclusions*. Tokyo: Yokendo; 1993.
20. Taha A, Sofronis P. A micromechanics approach to the study of hydrogen transport and embrittlement. *Eng Fract Mech*. 2001;68:803-837.
21. Furuya Y, Mataoka S, Abe T, Yamaguchi K. Gigacyclic fatigue properties for high-strength low-alloy steel at 100 Hz, 600 Hz and 20 kHz. *Scripta Mater*. 2002;46:157-162.
22. Pineau A, Antolovich S. Probabilistic approaches to fatigue with special emphasis on initiation from inclusions. *Int J Fatigue*. 2016;93(Part 2):422-434.
23. Chapetti MD, Tagawa T, Miyata T. Ultra-long cycle fatigue of high strength carbon steels. Part II: estimation of fatigue limit for failure from internal inclusions. *Mater Sci Eng Mat Sci Eng A*. 2003;356:236-244.
24. Frost NE, Pook LP, Danton K. A fracture mechanics analysis of fatigue crack growth data for various materials. *Eng Fract Mechanics*. 1971;3:109-126.
25. Kuroshima Y, Harada S (2001). Fatigue crack growth mechanism of high strength steel in gigacyclic fatigue regime. Proceedings of the Int. Conf. Fatigue in the very high cycle regime. Proceedings of the Int. Conf. Fatigue in the very high cycle regime, 229-236.
26. Tanaka K, Akiniwa Y. Fatigue crack propagation behaviour derived from S-N data in very high cycle regime. *Fatigue Fract Eng Mater Struct*. 2002;25:775-784.
27. Spriesterbach D, Brodyanski A, Lösch J, Kopnarski M, Kerscher E. Very high cycle fatigue of high strength steels: crack initiation by FGA formation investigated at artificial defects. *Procedia Structural Integrity*. 2016;2:1101-1108.
28. Juvonen P (2004). Effects of non-metallic inclusions on fatigue properties of calcium treated steels. PhD thesis, Helsinki University of Technology, Department of Mechanical Engineering.
29. Nishijima S, Tanaka K, Sumiyoshi H. The defect size determining the fatigue limits of steels. In: *Advances in Fracture Research (Fracture 84)*. Vol.3 New Delhi, India: Pergamon Press Ltd, Oxford; 1984:1719-1726.
30. Melander A, Ölund P. Detrimental effect of nitride and aluminium oxide inclusions on fatigue life in rotating bending of bearing steels. *Mater Sci Technol*. 1999;15(5):555-562.
31. Brooksbank D, Andrews KW. Stress fields around inclusions and their relation to mechanical properties. *Journal of the Iron and Steel Institute*. 1972;210:246-255.
32. Brooksbank D, Andrews KW. Thermal expansion of some inclusions found in steels and relation to tessellated stresses. *Journal of the Iron and Steel Institute*. 1968;206:595-599.
33. Brooksbank D, Andrews KW. Tesselated stresses associated with some inclusions in steels. *Journal of the Iron and Steel Institute*. 1969;207:474-483.
34. Brooksbank D. Thermal expansion of calcium aluminate inclusions and relation to tessellated stresses. *Journal of the Iron and Steel Institute*. 1970;208:495-499.
35. Melander A, Gustavsson A. An FEM study of driving forces of short cracks at inclusions in hard steels. *Int J Fatigue*. 1996;18:389-399.
36. Lemaitre J, Chaboche JL. *Mechanics of Solid Materials*. Cambridge, UK: University Press; 1994.
37. Brassart L, Doghri I, Delannay L. Homogenization of elasto-plastic composites coupled with a nonlinear finite element analysis of the equivalent inclusion problem. *Int J Solids Struct*. 2010; 47(Issue 5):716-729.
38. Guo S, Kang G, Zhang J. A cyclic visco-plastic constitutive model for time-dependent ratchetting of particle-reinforced metal matrix composites. *Int J Plasticity*. 2013;40:101-125.
39. Fleming WJ, Temis JM. Numerical simulation of cyclic plasticity and damage of an aluminium metal matrix composite with particulate SiC inclusions. *Int J Fat*. 2002;24(Issue 10):1079-1088.
40. Paul SK. Numerical models of plastic zones and associated deformations for elliptical inclusions in remote elastic loading-unloading with different R-ratios. *Eng Fract Mechanics*. 2016;152:72-80.
41. http://www.zset-software.com.
42. Besson J, Cailletaud G, Chaboche JL, Forest S, Blétry M. Nonlinear mechanics of materials. In: *Solid Mechanics and Its Applications*, 167, 433. Berlin, Germany: Springer; 2009.
43. Chaboche JL, Kanouté P, Azzouz F. Cyclic inelastic constitutive equations and their impact on the fatigue life predictions. *Int J Plasticity*. 2012;35:44-66.
44. Van Swam LF, Pelloux RM, Grant NJ. Fatigue behavior of maraging steel 300. *Met Trans A*. 1975;6:45-54.
45. Flouriot S, Forest S, Remy L. Strain localization phenomena under cyclic loading: application to fatigue of single crystals. *Comput Mat Sci*. 2003;26:61-70.
46. Papakyriacou M, Mayer H, Pypen C, Plink H, Stanzl-Tschegg S. Influence of loading frequency on high cycle fatigue properties of bcc and hcp metals. *Mater Sci Eng*. 2001;A308:143-152.
47. Bathias C. There is no infinite fatigue life in metallic materials. *Fatigue Fract Eng Mater Struct*. 1999;22:559-565.

How to cite this article: Pineau A, Forest S. Effects of inclusions on the very high cycle fatigue behaviour of steels. *Fatigue Fract Eng Mater Struct*. 2017;40:1694–1707. https://doi.org/10.1111/ffe.12649